Multiphysics Analysis of Carbon Composite Structural Batteries

Atharva Gujrathi
Undergraduate Member, Daniel Guggenheim School of Aerospace Engineering
Georgia Institute of Technology, Atlanta, GA
AIAA Student Member #1603243

Carbon composites have been a recent but increasingly important commodity in the field of aerospace engineering, with a drastic rise over the last 10-15 years. Carbon fiber structures typically come in the form of layers, or plies. This is done to enhance the tensile strengths in all planar directions, which carbon fiber has a naturally high capability of doing so. Each ply has its own fibers of composite material, which can differ in dimension and/or properties. To bind and shape these fibers together while allowing the transfer of loads between them, a matrix layer is often input in the middle of the plies. This paper utilizes an important but often overlooked characteristic of carbon fiber structures: electrical conduction. The basic properties of each ply type are shown to have non-zero electrical conductance; paired with a naturally conductive lithium-alloy matrix layer, these plies can create a structural battery. From this principle, a multiphysics model is created that analyzes a voltage differential in each battery (electrical), along with some atmospheric conduction (thermal) to determine the deformation of each battery due to the input voltage (structural). Structural batteries can act simultaneously as supports with mechanical integrity as well as storage of electrochemical energy. This allows for both weight reduction and cost-saving in aerospace applications such as UAVs and aircraft. This paper intends to detail the properties of multiple ply types, the setup of the multiphysics model, and the results and comparisons of each architecture.

I. Nomenclature

CNT	=	Carbon Nanotubes
CFRP	=	Carbon Fiber Reinforced Polymer
FEA	=	Finite Element Analysis
VAM	=	Variational Asymptotic Method
SBE	=	Structural Battery Electrode

II. Introduction and Background

This paper intends to explore the analysis of carbon composites natural property of electrical conduction, which has not been researched to the depth as has its mechanical and thermal properties. Carbon fibers usually come in plies, or layers, which are bonded together. This structure allows for planar tensile and compressive strengths, and the transfer or thermoelectric loads. Each ply, typically has a matrix layer inputted into the middle of the plies. This matrix layer can be made of thermosetting plastics or metal alloys to allow for enhancement of the carbon fiber properties.

Each specific sequence of plies and matrices is called an architecture. Typically, architectures come in odd number layers, such as 3, 5, 7, and 11, in order to build maximum tensile strengths and enhance each layer's individual properties. The fibers are placed in varying primary angles, typically in increments of 45° or 30° in order to maximize planar tensile loading.

In order to analyze carbon composites structures, it is best to use a FEA model, preferably a multiphysics capable software. FEA modeling allows for the identification of the effects from various types of loads in an assembly through the form of numerical solutions applied at a node. For the purpose of this research, Ansys 2023 R1 was selected. Ansys Workbench was used to manage overall layout of the model, while Ansys Mechanical was used to run the calculations and simulations.

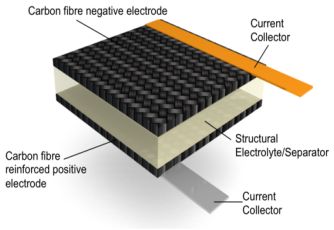

Fig. 1 Structural Battery Layout

The structural batteries, which comprise of carbon fiber plies around an electrically-conductive matrix layer, that are specifically explored in this paper are laminated structural electrodes. Each battery architecture is placed in a sandwich layout comprised of a lithium-ion matrix, which is known as the structural battery electrode (SBE)[1] layer surrounded by carbon fiber plies. This allows for both load bearing and the ability to transfer and store electrochemical energy. One of the main ply types examined in this is the carbon fiber with the addition of Carbon Nanotubes, or CNTs, as a coating reinforcement. These CNTs allow for maximization of the thermoelectric properties of carbon fiber and enhance other qualities, including corrosion protection, flexibility, and high strength-to-weight ratio[2]. The goal of this research was to analyze the incorporation of CNTs into carbon fiber plies, which make fuzzy fibers, and the effect from its placement on the battery anode. These fuzzy fibers were then compared with carbon fiber reinforced polymers (CFRPs) to determine how CNTs help enhance the thermoelectric properties. This paper details the properties of each type of ply obtained, the setup of the multiphysics Ansys model, and the results and comparisons with and without CNTs into the architecture.

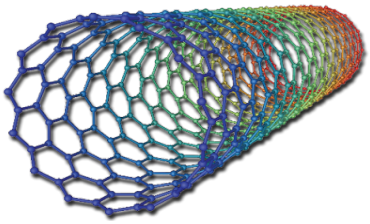

Fig. 2 Carbon Nanotubes Structural Layout

III. Architecture and Properties

This project examines 3 different battery architectures: one each with 3, 5, and 7 layers total. The first architecture incorporates a CFRP layer, a fuzzy fiber reinforced layer, and a matrix layer, with the matrix acting as a separator between the carbon fibers. The 2nd and 3rd architectures utilize reinforcement plies on the outsides of the ply cross-section. The cross-section for each architecture is shown in Figure 3.

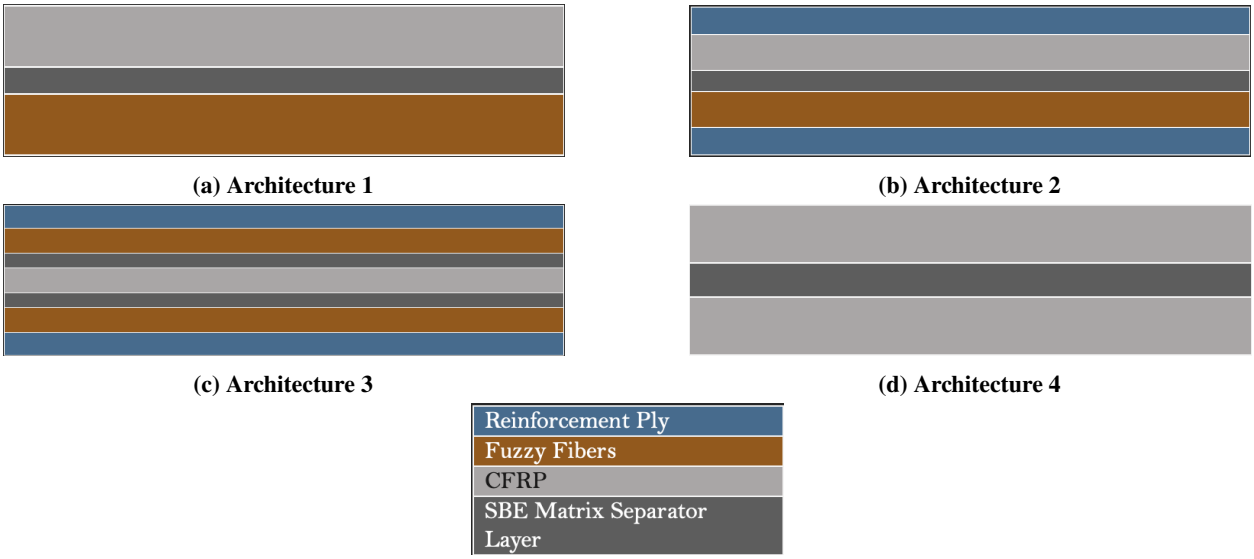

(a) Architecture 1

(b) Architecture 2

(c) Architecture 3

(d) Architecture 4

(e) Ply Legend

Fig. 3 Battery Architectures and Legend

The thicknesses of each ply type is detailed in Table 1.

Table 1 Ply Thicknesses

Ply Type	Thickness	Units
Matrix Separator	15	μm
CFRP	140	μm
Fuzzy Fiber Reinforced Ply	140	μm
Reinforcement Ply	100	μm

Each architecture had an overall width of 90mm and a length of 34mm. All architectures were created as an assembly model in SolidWorks CAD software and then imported into Ansys Workbench. A final architecture that replaces Fuzzy Fibers with CFRP was created to compare the addition of CNTs, with the overall dimensions kept the same.

Each ply type had different properties that were used in the Ansys model. The main properties of concern were strengths and conductivities of each ply. Based on the analytical homogenization models like the Halpin-Tsai model for mechanical properties and Self Consistent Theory for electrical properties, the effective properties of the composite laminates used in the current work have been determined. The volume fractions of the CFRPs and fuzzy fiber reinforced plies were taken to be 0.6. In the individual fuzzy fibers, the volume fraction of CNTs was 0.5. Variational Asymptotic Method (VAM) - based homogenization was used to estimate the effective properties of the singular fuzzy fibers. Table 2 lists all electrical, thermal, and structural properties used in the model.[3][4][5][6]

The assembly method used to create each architecture allowed the input of properties as separate entities. This kept each element in the model as a solid body rather than a shelled extrusion, which helped avoid program errors in Ansys.

IV. Ansys Model Setup

After importing the geometry into Ansys Mechanical, the workflow of the mesh construction was needed. Meshing refers to the process of dividing a geometric model into a large number of small, finite-sized elements. With meshing, the governing calculations and partial differential equations are applied to each individual cell. A surface mesh was constructed for this simple geometry, which breaks up the surface of the model geometry into its designated element sizes. The mesh was kept at a size of 1.5mm per cell. This allowed for the number of elements for each architecture to be in the ten-thousands. Since the overall structure is a rectangular prism, no complications in meshing structures were

Table 2 Electrical, Thermal, and Structural Properties of Each Ply Type

Property	CFRP	Fuzzy Fibers	Matrix Layer	Reinforcement Ply
Electrical Properties				
Isotropic Resistivity (Ωm)	$1.400 \cdot 10^{-5}$	$9.804 \cdot 10^{-6}$	66.667	N/A
Thermal Properties				
Isotropic Thermal Conductivity (W)	10.000	445.480	0.260	0.635
Coefficient of Thermal Expansion (K^-1)	$-5.600 \cdot 10^{-7}$	$-1 \cdot 10-6$	$-4.6 \cdot 10^{-5}$	N/A
Specific Heat with Constant Pressure ($JkgK$)	1040.000	1100.000	1670.000	750.610
Structural Properties				
Density (g/cm^3)	1.810	1.900	1.123	1.500
Ply Type	Isotropic	Isotropic	N/A	Isotropic
Young's Modulus (GPa)	114.400	97.663	0.600	11.520
Poisson's Ratio	0.311	0.300	0.300	0.280
Bulk Modulus (GPa)	100.780	81.386	0.500	8.727
Shear Modulus (GPa)	43.637	37.563	0.231	4.500

found in any architecture. The different materials associated with the different plies are defined in the setup phase of the model along with the mesh.

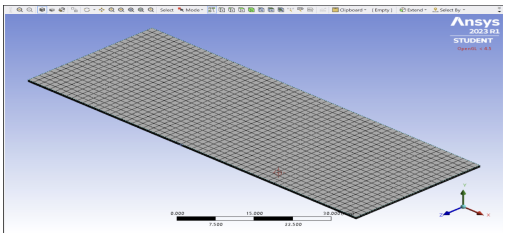

(a) Mesh

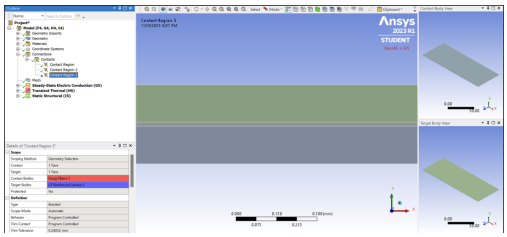

(b) Contact Region Settings

Fig. 4 General Mesh and Contact Region for Architectures

A. Electrical Settings

Analysis Settings: The total number of time steps was set to 10, with each interval being 1 second long.

Initial Conditions: Contact Regions between non-adjacent plies was suppressed. This prevented any unnecessary interference between the layers that distorted the thermal generation and deformation values.

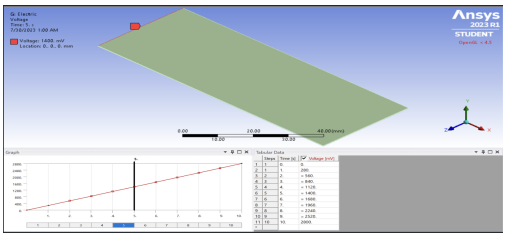

(a) Cathode Voltage Initial Conditions

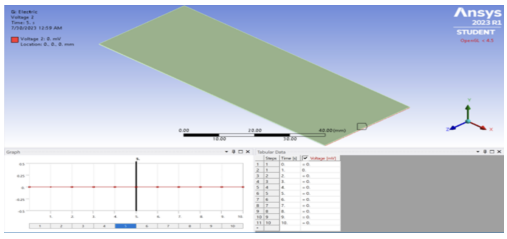

(b) Anode Voltage Initial Conditions

Fig. 5 Initial Electrical Conditions

B. Thermal Settings

Analysis Settings: Like the electrical analysis, the number of time steps were set to 10, with each sub-step being 1 second.

Initial Conditions: A convection unit across the top face was placed on each architecture. The value for the film coefficient across this face was placed at $3 \cdot 10^{-4} W/(mm^2 °C)$. The initial temperature setting for analysis was set at $22°C$, or standard room temperature.

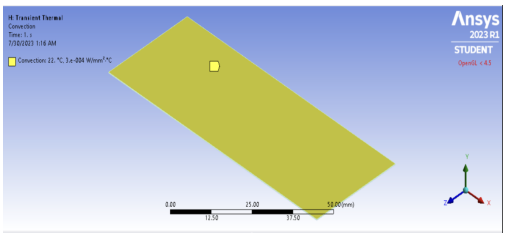

Fig. 6 Initial Thermal Conditions

C. Structural Settings

Analysis Settings: Like the electrical and thermal analysis portions, the number of time steps were set to 10, with each sub-step being 1 second.

Initial Conditions: For each architecture, different fixed supports were placed. The 1st architecture kept 1 fixed support at the faces of the +X axis. The 2nd architecture had 2 fixed supports at the + and – X axis faces, and the 3rd architecture had fixed supports at all 4 sides at their top edges.

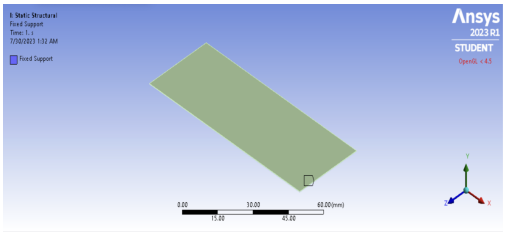

Fig. 7 Initial Structural Conditions

V. Results

A. Architecture 1

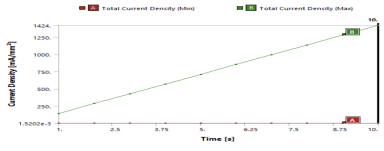

(a) Current Density (mA/mm^2) vs Time (s)

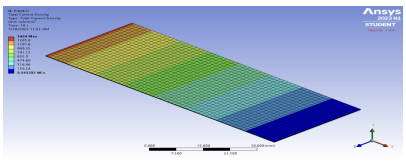

(b) Current Density

Steps	Time [s]	[A] Total Current Density (Min) [mA/mm²]	[B] Total Current Density (Max) [mA/mm²]
1	1.	1.5202e-003	142.4
2	2.	3.0404e-003	284.8
3	3.	4.5605e-003	427.2
4	4.	6.0807e-003	569.61
5	5.	7.6009e-003	712.01
6	6.	9.1211e-003	854.41
7	7.	1.0641e-002	996.81
8	8.	1.2161e-002	1139.2
9	9.	1.3682e-002	1281.6
10	10.	1.5202e-002	1424.

(c) Current Density Table

Fig. 8 Current Density Results of Architecture 1

The current density results were expected, as a linear relationship between current density was observed between the cathode and anode.

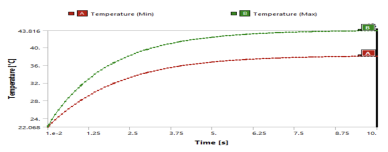

(a) Temperature $°C$ vs Time (s)

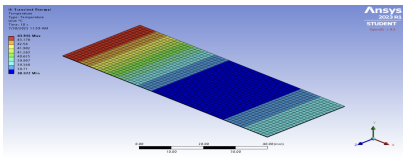

(b) Temperature

Steps	Time [s]	Temperature (Min) [°C]	Temperature (Max) [°C]
1	1	28.043	31.358
2	2	31.894	36.529
3	3	34.313	39.591
4	4	35.814	41.302
5	5	36.739	42.356
6	6	37.306	42.988
7	7	37.652	43.367
8	8	37.864	43.595
9	9	37.993	43.733
10	10	38.072	43.816

(c) Temperature Table

Fig. 9 Temperature Results of Architecture 1

The temperature doesn't correlate linearly like the current density does, as seen in the graph and table. The average temperature varies non-linearly with time, and it starts leveling out at around 7.5 seconds.

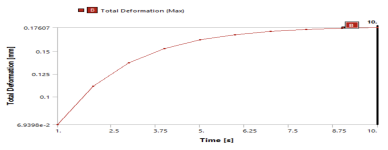

(a) Total Deformation (mm) vs Time (s)

Steps	Time [s]	[B] Total Deformation (Max) [mm]
1	1.	6.9398e-002
2	2.	0.11151
3	3.	0.1372
4	4.	0.15286
5	5.	0.16242
6	6.	0.16824
7	7.	0.17179
8	8.	0.17395
9	9.	0.17527
10	10.	0.17607

(b) Total Deformation Table

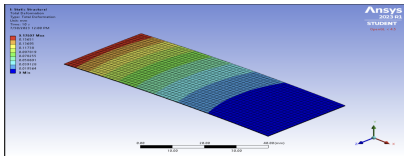

(c) Isometric View of Total Deformation

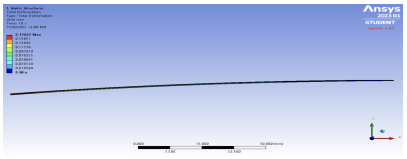

(d) Side View of Total Deformation

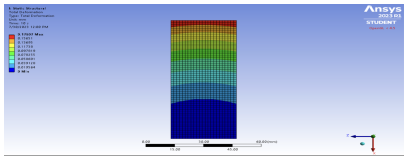

(e) Top View of Total Deformation

Fig. 10 Total Deformations Results of Architecture 1

The boundary condition applied to this architecture was a fixed support at the +X face. This gave a deformation curve that was highest at the cathode, as expected. Again, a non-linear deformation vs. time curve is seen, similar to temperature. The maximum deformation was about 0.17mm.

B. Architecture 2

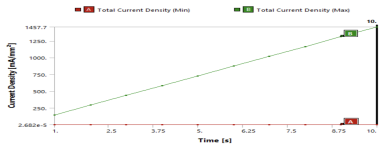

(a) Current Density (mA/mm^2) vs Time (s)

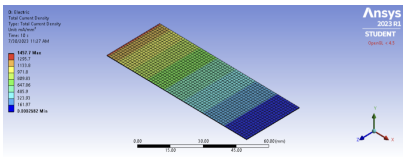

(b) Current Density

Steps	Time [s]	[A] Total Current Density (Min) [mA/mm²]	[B] Total Current Density (Max) [mA/mm²]
1	1.	2.682e-005	145.77
2	2.	5.364e-005	291.54
3	3.	8.046e-005	437.31
4	4.	1.0728e-004	583.08
5	5.	1.341e-004	728.85
6	6.	1.6092e-004	874.62
7	7.	1.8774e-004	1020.4
8	8.	2.1456e-004	1166.2
9	9.	2.4138e-004	1311.9
10	10.	2.682e-004	1457.7

(c) Current Density Table

Fig. 11 Current Density Results of Architecture 2

The current density results were expected, as a linear relationship between current density was observed between the cathode and anode. However, it was spaced differently than architecture 1.

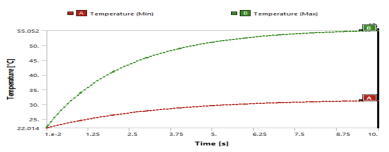

(a) Temperature $°C$ vs Time (s)

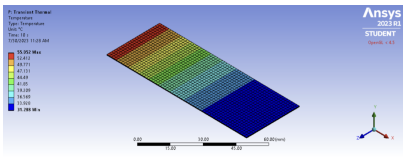

(b) Temperature

Steps	Time [s]	Temperature (Min) [°C]	Temperature (Max) [°C]
1	1	24.494	33.729
2	2	26.370	41.000
3	3	27.766	45.770
4	4	28.805	48.956
5	5	29.578	51.109
6	6	30.151	52.573
7	7	30.576	53.573
8	8	30.889	54.257
9	9	31.119	54.728
10	10	31.288	55.052

(c) Temperature Table

Fig. 12 Temperature Results of Architecture 2

The temperature doesn't correlate linearly like the current density does, as seen in the graph and table. The average temperature varies non-linearly with time, and it starts leveling out at around 7.5 seconds, similar to the first architecture.

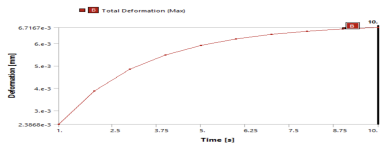

(a) Total Deformation (mm) vs Time (s)

Steps	Time [s]	[B] Total Deformation (Max) [mm]
1	1.	2.3868e-003
2	2.	3.8798e-003
3	3.	4.8451e-003
4	4.	5.4841e-003
5	5.	5.9146e-003
6	6.	6.2083e-003
7	7.	6.4106e-003
8	8.	6.5508e-003
9	9.	6.6484e-003
10	10.	6.7167e-003

(b) Total Deformation Table

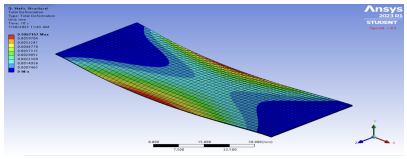

(c) Isometric View of Total Deformation

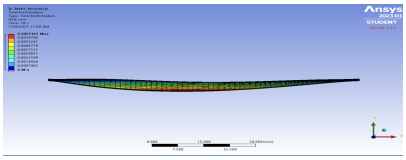

(d) Side View of Total Deformation

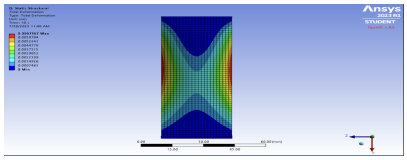

(e) Top View of Total Deformation

Fig. 13 Total Deformations Results for Architecture 2

The boundary condition applied to this architecture was a fixed support at the + and -X faces. This gave a deformation curve that was highest along the + and - Y faces, closer to the cathode than anode. Again, a non-linear deformation vs. time curve is seen, similar to temperature. The maximum deformation was about 0.06mm. This was expected to be less than Architecture 1 because of the increased layers of supporting plies.

C. Architecture 3

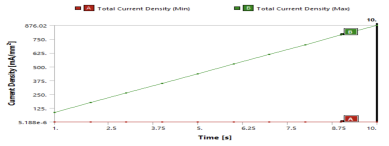

(a) Current Density (mA/mm^2) vs Time (s)

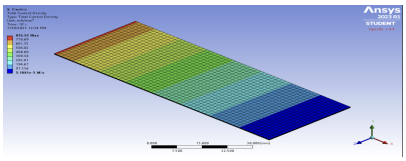

(b) Current Density

Steps	Time [s]	[A] Total Current Density (Min) [mA/mm²]	[B] Total Current Density (Max) [mA/mm²]
1	1.	5.188e-006	87.602
2	2.	1.0376e-005	175.2
3	3.	1.5564e-005	262.81
4	4.	2.0752e-005	350.41
5	5.	2.594e-005	438.01
6	6.	3.1128e-005	525.61
7	7.	3.6317e-005	613.22
8	8.	4.1504e-005	700.82
9	9.	4.6693e-005	788.42
10	10.	5.1881e-005	876.02

(c) Current Density Table

Fig. 14 Current Density Results of Architecture 3

The current density results were expected, as a linear relationship between current density was observed between the cathode and anode. The spacing was similar to that of architecture 2.

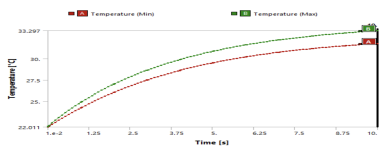

(a) Temperature $°C$ vs Time (s)

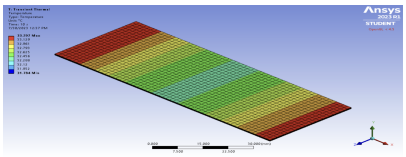

(b) Temperature

Steps	Time [s]	Temperature (Min) [°C]	Temperature (Max) [°C]
1	1	24.242	24.892
2	2	26.056	27.022
3	3	27.496	28.649
4	4	28.632	29.903
5	5	29.524	30.873
6	6	30.221	31.625
7	7	30.767	32.211
8	8	31.192	32.666
9	9	31.525	33.021
10	10	31.784	33.297

(c) Temperature Table

Fig. 15 Temperature Results of Architecture 3

The temperature varied greatly with this architecture, with the highest temperatures found at the cathode and anode. This architecture didn't have the same leveling out of temperature as seen before, so more time steps could've helped to gauge the full profile.

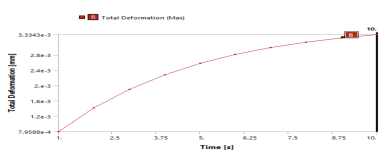

(a) Total Deformation (mm) vs Time (s)

Steps	Time [s]	[B] Total Deformation (Max) [mm]
1	1.	7.9588e-004
2	2.	1.4172e-003
3	3.	1.9042e-003
4	4.	2.2851e-003
5	5.	2.5828e-003
6	6.	2.8153e-003
7	7.	2.9967e-003
8	8.	3.1381e-003
9	9.	3.2484e-003
10	10.	3.3343e-003

(b) Total Deformation Table

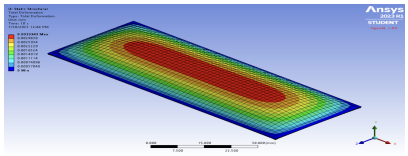

(c) Isometric View of Total Deformation

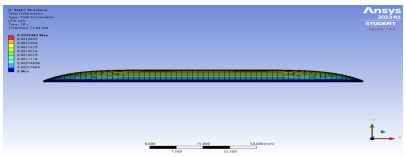

(d) Side View of Total Deformation

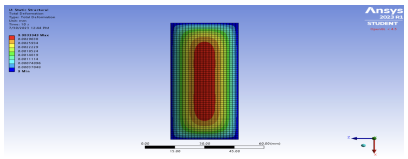

(e) Top View of Total Deformation

Fig. 16 Total Deformations Results for Architecture 3

The boundary condition applied to this architecture was a fixed support at the + and -X and -Y faces. This gave a deformation curve that was highest in the center, both in the X and Y plane. Again, a non-linear deformation vs. time curve is seen, similar to temperature. The maximum deformation was about 0.03mm. This was expected to be less than Architecture 2 as well because of the further increase in layers of supporting plies.

D. Architecture 4

In order to compare the effectiveness of the CNTs added to create the fuzzy fibers, the exact same analysis was conducted on the first architecture, except the fuzzy fiber reinforced layer was replaced by a CFRP layer. The same electrical, thermal, and structural initial conditions were kept.

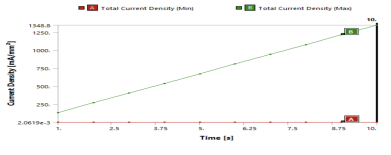

(a) Current Density (mA/mm^2) vs Time (s)

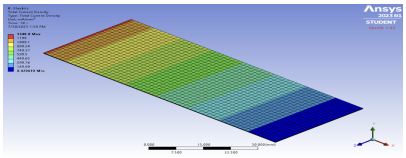

(b) Current Density

Steps	Time [s]	[A] Total Current Density (Min) [mA/mm²]	[B] Total Current Density (Max) [mA/mm²]
1	1.	2.0619e-003	134.88
2	2.	4.1238e-003	269.77
3	3.	6.1858e-003	404.65
4	4.	8.2477e-003	539.54
5	5.	1.031e-002	674.42
6	6.	1.2372e-002	809.31
7	7.	1.4433e-002	944.19
8	8.	1.6495e-002	1079.1
9	9.	1.8557e-002	1214.
10	10.	2.0619e-002	1348.8

(c) Current Density Table

Fig. 17 Current Density Results of Architecture 4

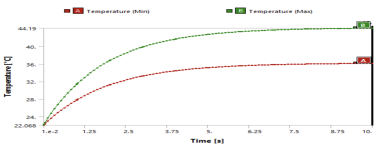

(a) Temperature $°C$ vs Time (s)

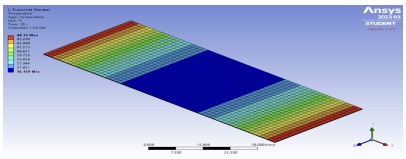

(b) Temperature

Steps	Time [s]	Temperature (Min) [°C]	Temperature (Max) [°C]
1	1	27.778	31.849
2	2	31.212	36.724
3	3	33.252	39.857
4	4	34.464	41.691
5	5	35.184	42.766
6	6	35.611	43.397
7	7	35.865	43.768
8	8	36.016	43.986
9	9	36.106	44.115
10	10	36.159	44.190

(c) Temperature Table

Fig. 18 Temperature Results of Architecture 4

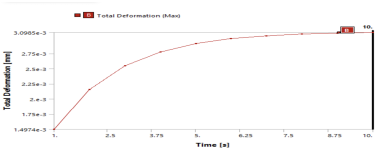

(a) Total Deformation (mm) vs Time (s)

Steps	Time [s]	[B] Total Deformation (Max) [mm]
1	1.	1.4974e-003
2	2.	2.1557e-003
3	3.	2.5459e-003
4	4.	2.7771e-003
5	5.	2.9141e-003
6	6.	2.9952e-003
7	7.	3.0432e-003
8	8.	3.0717e-003
9	9.	3.0885e-003
10	10.	3.0985e-003

(b) Total Deformation Table

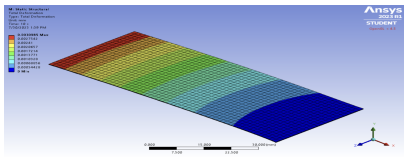

(c) Isometric View of Total Deformation

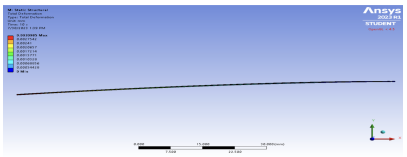

(d) Side View of Total Deformation

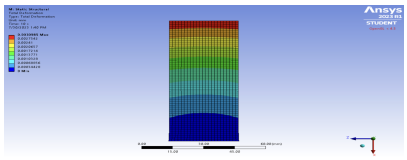

(e) Top View of Total Deformation

Fig. 19 Total Deformations Results for Architecture 4

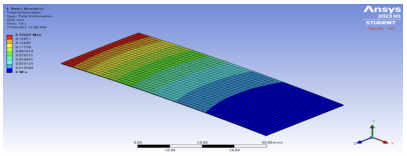

(a) Total Deformation with CFRPs

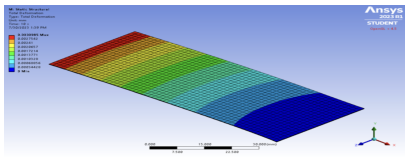

(b) Total Deformation with CNT Fuzzy Fibers

Fig. 20 Total Deformation Comparison between CFRPs and CNT Fuzzy Fibers

Because of the higher coefficient of thermal expansion for the fuzzy fibers, the deformation was higher on the initial architecture vs. the CFRP-only architecture. However, the architecture with the fuzzy fibers had a higher range of current density than it's CFRP counterpart.

VI. Discussion and Conclusion

In principle, it is clear that inputting a voltage differential in carbon composites creates thermal and structural stresses into each battery architecture that causes thermal expansion, and deformation in the batteries. However, the deformation that was created was small in all batteries, with the max deformation ranging from 3 μm to 17 μm, depending on architecture. Because of the limited deformation, scalability of the battery architectures is possible, as these deformations should not cause delamination and/or structural failures across the architectures.

Another key observation was that deformation decreased as the ply layers increased. This was expected, as the reinforcement plies were expanded very little from thermal generation. However, the temperature and current density shapes generated by each battery varied, as generally non-linear effects took over.

The CFRP-only Architecture 1 managed to yield a lower deformation range because of the coefficient of thermal expansion of the different fibers. Because the CNTs in Fuzzy Fibers increase CTE, the deformation in the initial architecture increased. However, the additional properties, such as increased thermal conduction, allowed for a more homogeneous thermal profile (5 °C) variance as compared to the CFRP-only architecture (8 °C).

Overall, the model structure can be adjusted by only changing the property values assigned to the various plies. Because of the ambiguity on some property values on various plies, there is yet to be final confirmation of the exact numbers yielded by the simulations. For example, a specific heat of $1100 J/(kgK)$ and a coefficient of thermal expansion of $-1^{-6}K^{-1}$ for the fuzzy fibers were estimated with some data about their relationships with the CFRP plies [7]. Because of this, some results (even the comparisons between Battery Architecture 1 and 4) may not be fully conclusive.

VII. Future Scope

This analysis of each structural battery architecture involved evaluating the electrical, thermal, and structural stresses of inputting a single voltage differential into the battery. Many factors that were not considered in the making of the model could be used as a scope for future research on this particular project. Keeping the architecture shapes, environment settings, and initial conditions constant, key areas to analyze in the future include, but are not limited to:

- Nonlinear analysis including failure analysis
- Delamination inside each battery architecture
- Thermal stress concentration
- Time-variance of electrical and thermal inputs
- Support types

Nonlinear analysis and delamination help answer key questions about the nature of carbon fiber that could not be explored using a simple assembly model in Ansys. This will allow us to see if the 3 – 17 micrometer deformation just causes a slight bend or any major structural issues. The types of bonds between the layers may be adjusted to incorporate this analysis.

Thermal stress concentration was not explored in this research, however the calculations for heat flux, thermal stress, and thermal strain were completed. These results could have been used as indicators on the weak points in each battery architecture, which would give key information about failure areas and more.

Time-variance on both electrical and thermal settings is a possible avenue to explore if repeated or varying loads can cause deformation and stresses over time that lead to failure, even if the loads are kept relatively low. The varying conditions can also show the true effectiveness of the ply properties.

Lastly, different support types should also be explored, as varying results may occur based on fixed supports being placed on faces or edges. Other types of supports may be beneficial as well, including remote displacements or nodal supports.

Acknowledgments

The author Atharva Gujrathi would like to thank Renuka Sahu, PhD at the NMCAD Lab, and Dr. Dineshkumar Harursampath, Aerospace Engineering for guidance and instruction throughout the process of developing the model and writing the research report. The author would like to thank the Georgia Tech Aerospace Engineering India Study Abroad program for providing this opportunity. The author would also like to thank the Aerospace Engineering department of the Indian Institute of Science in Bengaluru, India, for hosting Georgia Tech AE and providing the facilities necessary to conduct this research.

References

[1] N. Ihrner, F. S. D. Z. M. J., W. Johannisson, "Structural lithium ion battery electrolytes via reaction induced phase-separation," *Journals of Material Chemistry A*, Vol. 5, 2017, pp. 44–46. https://doi.org/110.1039/C7TA04684G.

[2] Waqar Ahmed, V. D. K. S., Abdelbary Elhissi, *Emerging Nanotechnologies in Dentistry*, 2nd ed., William Andrew Applied Science Publishers, New York, 2018, Chap. 18.

[3] Baker, J. D., "Thermal Characterization Of Carbon Composites," *Aggie Digital Collections and Scholarship*, 2011.

[4] Pauline Tranchard, S. D. B. E., Fabienne Samyn, and Bourbigot, S., "Modelling Behaviour of a Carbon Epoxy Composite Exposed to Fire: Part I—Characterisation of Thermophysical Properties," *Materials*, Vol. 10, 2017, p. 494. https://doi.org/10.3390/ma10050494.

[5] Suna, B., "Design and Analysis of Laminated Composite Materials," 2011.

[6] "T800H Intermediate Modulus Carbon Fiber," https://www.toraycma.com/wp-content/uploads/T800H-Technical-Data-Sheet-1.pdf.pdf, 2018.

[7] Shailesh I. Kundawal, M. R., "Thermoelastic Properties of a Novel Fuzzy Fiber-Reinforced Composite," *Journals of Applied Medicines*, Vol. 6, 2013, p. 80. https://doi.org/10.1115/1.4023691.